



# Copper chromite decorated on nitrogen-doped graphene aerogel as an efficient catalyst for thermal decomposition of ammonium perchlorate particles

Seyed Ghorban Hosseini<sup>1</sup> · Zahra Khodadadipoor<sup>1</sup> · Mojtaba Mahyari<sup>1</sup> · Javad Mohebbi Zinab<sup>1</sup>

Received: 21 December 2018 / Accepted: 15 April 2019

© Akadémiai Kiadó, Budapest, Hungary 2019

## Abstract

In this study, CuCr<sub>2</sub>O<sub>4</sub> spinel (CCO) nanoparticles decorated on three-dimensional graphene networks were synthesized using hydrothermal method followed by a calcination process. The as-prepared material was characterized by different analysis methods and used for catalytic thermal decomposition of ammonium perchlorate particles (AP). For this purpose, CuCr<sub>2</sub>O<sub>4</sub>@GA/AP composites were fabricated by solvent/non-solvent (composite processing) and simple mixing methods. The catalytic effect of the as-prepared composites was investigated by differential scanning calorimetric and thermogravimetric (TG) analysis techniques. Owing to the synergistic effect of the spinel-structured copper chromite nanoparticles, high surface area of graphene aerogel and composite processing of AP, the high-temperature decomposition of AP in the presence of 4 mass% CuCr<sub>2</sub>O<sub>4</sub>@GA nanocomposite prepared by solvent/non-solvent method was reduced from 432 to 323 °C and the heat released ( $\Delta H$ ) from decomposition of AP was increased from 590 to 1760 J g<sup>-1</sup>.

**Keywords** CuCr<sub>2</sub>O<sub>4</sub> spinel nanoparticles · 3D GA · Ammonium perchlorate · Catalytic activity · Thermal decomposition

## Introduction

Ammonium perchlorate (AP) as a white crystalline substance is highly used in composite solid propellants as the most important oxidizer [1, 2] since the burning characteristics of the composite propellants are directly linked to the thermal decomposition property of AP [3, 4]. Therefore, the lower high-temperature decomposition (HTD) temperature and the higher apparent heat release cause a lower ignition delay time and a higher burning rate of composite propellants [5]. In the past decades, a variety of catalysts including metals and their oxides, complex oxides and composite catalysts have been explored to enhance decomposition efficiency of AP [6–9]. Copper chromium mixed oxides (CuCr<sub>2</sub>O<sub>4</sub>) as a *p*-type semiconducting oxide

have been used as an effective catalyst for thermal decomposition of AP [10, 11]. The high activity of copper chromite is related to the tetragonally distorted normal spinel structure [12]. Copper chromite nanoparticles have been prepared by several methods such as sol-gel, co-precipitation and hydrothermal [13, 14]. Several studies on the decomposition of AP in the presence of CuCr<sub>2</sub>O<sub>4</sub> produced through co-precipitation [15], thermal decomposition of copper ammonium chromate [16] and sol-gel [17] have been promisingly applied as burning rate catalysts.

Moreover, the catalytic performance of nanoparticles is very dependent on the specific surface area [18]. However, nanoscale materials tend to aggregate which resulted to decrease their catalytic activities [19]. In recent years, catalyst supports such as carbon nanotube, graphene, three-dimensional graphene and three-dimensional porous carbon have been developed to improve the catalytic activity of nanostructures for thermal decomposition of AP [20–23]. Among these, three-dimensional graphene-based frameworks (3D GFs) or graphene aerogels (GAs) with well-connected porous structures, high surface area, as well as good electrical and thermal conductivity have gained

✉ Seyed Ghorban Hosseini  
hosseinitol@yahoo.com

Mojtaba Mahyari  
m\_mahyari@sbu.ac.ir

<sup>1</sup> Department of Chemistry, Malek Ashtar University of Technology, P.O. Box 16765-3454, Tehran, Iran

much attention for catalytic application [24–26]. Compared to the limited surface area of graphene, 3D graphene exhibited many catalytic active sites due to its porous structure [27]. Moreover, its exothermic reaction with oxidizing products and electrical and thermal conductivity can accelerate thermal decomposition of AP [24].

On the other hand, the performance of the catalysts is attributed to the contact area between the catalysts and AP [28]. The preparation of superfine AP can improve contact and then lead to the higher catalytic activity. However, the preparation of superfine AP due to its nature of strong oxidant is very dangerous and challenging [29]. The preparation of nanocomposites of AP and the catalysts in comparison with those simple physical mixing has shown higher contact area and more catalytic active sites, resulting in the enhancement of their catalytic activity [30, 31]. Moreover, the structural features of catalysts, such as high surface area and porosity, also can enhance the catalytic activity through accelerating the adsorption and desorption of gas products during the thermal decomposition process of AP [32, 33]. In our previous work, we demonstrated that 3D N-GFs as support for copper oxide and Ni–Mn alloys could improve thermal decomposition of AP [34, 35].

Herein, in continuation of our effort for developing new catalysts supported on 3D graphene [34, 35], in the first stage, pure CuCr<sub>2</sub>O<sub>4</sub> NPs and CuCr<sub>2</sub>O<sub>4</sub>@GA nanocomposite were synthesized by hydrothermal route combined with the calcination process. In the next stage, nanocomposites of AP and CuCr<sub>2</sub>O<sub>4</sub>@GA were prepared by simple physical mixing and composite processing (solvent/non-solvent method). Furthermore, the catalytic effect of composites for the decomposition of ammonium perchlorate (AP) was investigated by DSC and TG analysis.

## Experimental

### Material and method

Chemical materials including natural graphite flake (99.8%, 325 mesh), copper nitrate (Cu(NO<sub>3</sub>)<sub>2</sub>·5H<sub>2</sub>O), chromium nitrate (Cr(NO<sub>3</sub>)<sub>3</sub>·9H<sub>2</sub>O), cetyl trimethyl ammonium bromide (CTAB), hydrazine, hydrogen peroxide, sulfuric acid, potassium permanganate, phosphorous pentoxide and ammonium hydroxide were purchased from Merck. Analytical reagent-grade NH<sub>4</sub>ClO<sub>4</sub> powder was obtained from Fluka. Methyl isobutyl ketone was purchased from Merck as non-solvent. All of the chemical materials were used without further purification. All solvents used were of reagent grade. All syntheses were carried out under ambient conditions. Deionized and double-distilled water were used in these experiments.

The X-ray diffraction analysis of the samples was performed with a PW1730 (Philips, Netherlands) diffractometer using Cu-K $\alpha$  radiation with a wavelength of 1.54060 Å to investigate the structure of GA, CuCr<sub>2</sub>O<sub>4</sub> NPs and CuCr<sub>2</sub>O<sub>4</sub>@GA nanocomposites. The diffraction patterns were recorded over a 2 $\theta$  range of 10°–80° at 40 kV and 40 mA with 0.05° step size. Field emission scanning electron microscopy (FE-SEM, EIGMA/VP) was employed to determine morphologies, particle size and coating quality of the samples. FT-IR spectra were recorded on a Nicolet 800 instrument using KBr in the range of 400–4500 cm<sup>-1</sup> to obtain the compositions of the samples. Raman spectra were carried out with Nd:YAG laser, TAKRAM P50C0R10, Tekسان. The Brunauer–Emmett–Teller (BET) surface area of CCO and CCO@GA samples were determined using a BELSORP-max surface detecting device by physisorption of N<sub>2</sub> at 77 K. The thermal decomposition analysis of the CuCr<sub>2</sub>O<sub>4</sub>@GA nanocomposite was performed by employing thermogravimetry–differential scanning calorimetry (TG-DSC) simultaneously in an STA-780 thermal analysis system under nitrogen atmosphere and with a heating rate of 10 °C min<sup>-1</sup>. The dispersion of CuCr<sub>2</sub>O<sub>4</sub>@GA in non-solvent and materials in solvents was carried out by the ultrasonic bath (LAB Sonic RP operating at 45 kHz).

### Preparation of CuCr<sub>2</sub>O<sub>4</sub> spinel nanoparticles

The CuCr<sub>2</sub>O<sub>4</sub> spinel nanoparticles were obtained by a hydrothermal method from copper and chromium nitrate with some modification [36]. In the first step, 2.3 g of Cu(NO<sub>3</sub>)<sub>2</sub>·3H<sub>2</sub>O and 7.5 g of Cr(NO<sub>3</sub>)<sub>3</sub>·9H<sub>2</sub>O with vigorous stirring are dissolved in 40 g deionized water to give a transparent dark blue homogeneous solution. Then, the pH of the solution was reached eight by gradual addition of a few drops of ammonia to the solution. An ethanolic solution (10%) of 2.6 g CTAB was added dropwise to form a gel followed by the addition of 0.6 g hydrazine to the well-stirred mixture at room temperature by vigorous stirring. All the reagents were added while maintaining the molar ratio of Cu:Cr:CTAB:H<sub>2</sub>O:hydrazine = 1:2:0.75:250:1. After stirring for 30 min, the produced homogeneous solution was sealed in a Teflon-lined stainless steel autoclave vessel at 180 °C for 24 h and then allowed to cool. The products as green fluffy solid precipitates were collected by centrifugation at 18,000 rpm and washed with water several times and dried in air at 120 °C, for ten h. In the next step, the collected products were calcined at 750 °C for 6 h in air to get CuCr<sub>2</sub>O<sub>4</sub> spinel nanoparticles.

## Preparation of graphene oxide (GO)

Graphene oxide (GO) was fabricated through the modified Hummers method [37]. Firstly, 1.00 g graphite powder, 0.75 g NaNO<sub>3</sub> and 130 mL of concentrated H<sub>2</sub>SO<sub>4</sub> were magnetically stirred in an ice bath. Under vigorous stirring, 3.00 g KMnO<sub>4</sub> was added slowly over about 1 h. The reaction mixture was stirred for 10 h in a water bath, 45 mL water was added, and the solution was stirred for 30 min at 90 °C. After that, 10 mL H<sub>2</sub>O<sub>2</sub> (30%) and 140 mL deionized water were added to the mixture and the color of solutions changed from dark brown to yellow. Then, the resulting precipitate was centrifuged at 3000 rpm for 40 min and washed with 1:10 HCl aqueous solution several times to remove metal ions, and the resulting sample was dried under vacuum at 60 °C for 3 days. The final sample was obtained as a GO brown powder.

## Preparation of graphene aerogel (GA)

Typically, GA was fabricated from GO suspension followed by freeze-drying process. According to our previous work, graphene aerogel (GA) was prepared with a combined hydrothermal and freeze-drying process from graphene oxide (GO). In a typical preparation method, GO was dispersed in water under ultrasonic vibration to reach a concentration to 1.5 mg mL<sup>-1</sup>. Then the mixture was poured into a Teflon-lined stainless steel autoclave (100 mL capacity). The autoclave was heated to 180 °C for 12 h. The as-prepared black hydrogel was freeze-dried overnight to form GA.

## Preparation of CCO@GA nanocomposite

In a typical experiment, the CCO powders which were previously obtained were mixed with the GA aqueous suspensions and ultrasonication for one h to obtain the stable mixed suspensions. In the next step, the mixed suspensions were transferred into a 50-mL Teflon-lined stainless steel autoclave vessel. After heated to 180 °C for three h, the CuCr<sub>2</sub>O<sub>4</sub>@GA nanocomposite materials were obtained. After cooling down, the solutions were washed with deionized water by distilled water several times and dried at 60 °C in an oven for 12 h.

## Preparation of AP/(CuCr<sub>2</sub>O<sub>4</sub> spinel NPs and CCO@GA)

To evaluate the catalytic activity of the as-prepared CuCr<sub>2</sub>O<sub>4</sub> NPs, CuCr<sub>2</sub>O<sub>4</sub>@GA nanocomposite and NH<sub>4</sub>ClO<sub>4</sub> (to produce composites), they were mixed by the simple mixing and solvent/non-solvent route. In this study,

water and methyl isobutyl ketone were chosen as the solvent and non-solvent, respectively. First, the CuCr<sub>2</sub>O<sub>4</sub> NPs were dispersed in 25 mL acetone by ultrasonication for 15 min. Also, AP was dissolved into the water to make a saturated solution at 80 °C. The saturated solution of AP was added dropwise into the CuCr<sub>2</sub>O<sub>4</sub> NPs to obtain a composite of CuCr<sub>2</sub>O<sub>4</sub>/AP. In this experiment, AP was mixed with the as-prepared catalyst at a mass ratio of 96:4. Then, the reaction lasted for several minutes until all the AP was deposited on the surface of the CuCr<sub>2</sub>O<sub>4</sub> particles. Finally, the coated particles (i.e., composites) were filtered and washed with 25 mL acetone as non-solvent three times and dried at ambient temperature.

## Result and discussion

### Characterization of structure, morphology and size of catalysts

Fourier transforms infrared spectroscopy (FT-IR) for investigation of the structure and the chemical bonds of the GA, CCO NPs and CCO@GA are shown in Fig. 1. According to Fig. 1a, the FT-IR of GA shows peaks around 1060 cm<sup>-1</sup> corresponding to C–O stretching vibration of epoxy group and 1710 cm<sup>-1</sup> corresponding to C=O stretching vibration of carboxyl group. Two small peaks around 2854 and 2927 cm<sup>-1</sup> attributed to asymmetric and symmetric CH stretching modes, respectively. FT-IR spectrum of CCO@GA nanocomposite (Fig. 1c) showed that peaks around 3421 cm<sup>-1</sup> attributed to OH<sup>-</sup> vibration and absorption peaks at 1718 cm<sup>-1</sup> and 1621 cm<sup>-1</sup> corresponded to the stretching vibrations of the double-bond C=O and C=C. Also, the two strong peaks at around 522 cm<sup>-1</sup> and 611 cm<sup>-1</sup> corresponded to the vibration of

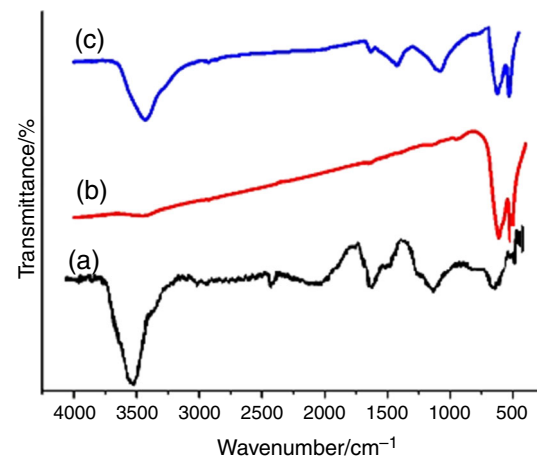


**Fig. 1** FT-IR spectra of GA (a), CCO NPs (b) and CCO@GA nanocomposite (c)

the group of  $\text{Cr}_2\text{O}_4^{2-}$  in the  $\text{CuCr}_2\text{O}_4$ . This confirmed that  $\text{CuCr}_2\text{O}_4$  was produced.

The phase structure and purity of the as-prepared samples were investigated by XRD pattern (Fig. 2). The XRD pattern of GA depicted a broad diffraction peak at  $22.5^\circ$  (002) plane that related to the interlayer spacing of  $0.395\text{ nm}$ . The diffraction peaks of CCO@GA at  $18.6^\circ$ ,  $29.6^\circ$ ,  $31.1^\circ$ ,  $35.2^\circ$ ,  $37.7^\circ$ ,  $56.2^\circ$  represent the crystal planes of (101), (200), (112), (211), (202), (321) of spinel structure (PDF card: 88-0110), respectively. In  $\text{CuCr}_2\text{O}_4$  structure, Cu and Cr occupied the tetrahedral and octahedral interstices, severally. Furthermore, the diffraction peak at around  $22.5^\circ$  corresponding to the (002) reflection of GA was observed. The average particle size of  $\text{CuCr}_2\text{O}_4$  spinel nanoparticle was determined using Debye–Scherrer equation (Eq. 1) [38] from the width half maxima of the line broadening attributed to the diffraction angle of  $35.16^\circ$

$$D = \frac{k\lambda}{\beta \cos \theta} \quad (1)$$

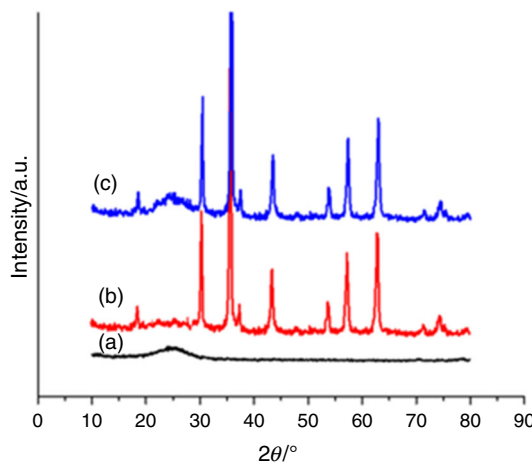
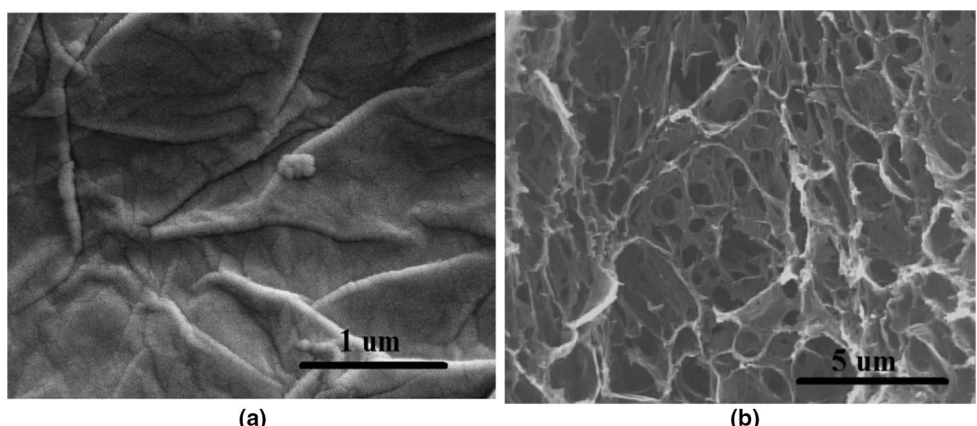


**Fig. 2** XRD patterns of GA (a), CCO NPs (b) and CCO@GA nanocomposite (c)

**Fig. 3** SEM images of GO (a) and GA (b)



where  $D$  is the particle size,  $k$  is a dimensionless shape factor and is equal to 0.9,  $\lambda$  is the wavelength of X-ray radiation,  $\beta$  is the full width at half maximum (FWHM) of the diffraction peak and  $\theta$  is the Bragg angle. The calculated average size of the particles was about 42 nm. Typical scanning electron microscopy (SEM) images of the suspended GO sheets and GA are shown in Fig. 3. As shown in Fig. 3a, SEM images revealed the exfoliated graphene sheets with lateral dimensions of several micrometers. Figure 3b shows 3D network structure with continuous macropores, and the sizes of pores range from a few hundred nanometers to several micrometers.

The morphology of the CCO NPs and CCO@GA products is shown in Fig. 4. As it is observed in Fig. 4a, the CCO nanoparticles with sphere-like shape and an average diameter of  $\sim 38\text{ nm}$  are unagglomerated and homogeneously distributed uniform particles which is in good agreement with the results of XRD analysis. It is noted that  $\text{CuCr}_2\text{O}_4$  spinel nanoparticle prepared by a hydrothermal method in the presence of CTAB surfactant owing to the assembly influence of the surfactant depicted a single-phase morphology. Furthermore, it was found that in the CCO@GA nanocomposite as shown in Fig. 4b–d, the CCO nanoparticles still retained their morphology and size as bare CCO nanoparticles. As shown in Fig. 3, CCO nanoparticles encapsulated within the graphene networks and wrapped to form the nanocomposite.

Moreover, the CCO@GA and GA were characterized by Raman spectroscopy. As shown in Fig. 5, typical Raman spectra of GA exhibit two intense Raman peaks: D band and G band. The peaks at  $1354$  and  $1590\text{ cm}^{-1}$  were assigned to the D and G bands. This causes the defects and the in-plane vibrations of the  $\text{sp}^2$  carbon atoms. Also, similar D and G bands were observed for CCO@GA nanocomposite. In general, the intensity ratios of the D and G bands ( $\text{ID}/\text{IG}$ ) displayed the graphitization degrees and the defects of carbon species. The value of  $\text{ID}/\text{IG}$  for the CCO@GA is smaller than graphene aerogel that indicated

**Fig. 4** FE-SEM images of CCO NPs (a) and CCO@GA nanocomposite (b–d)

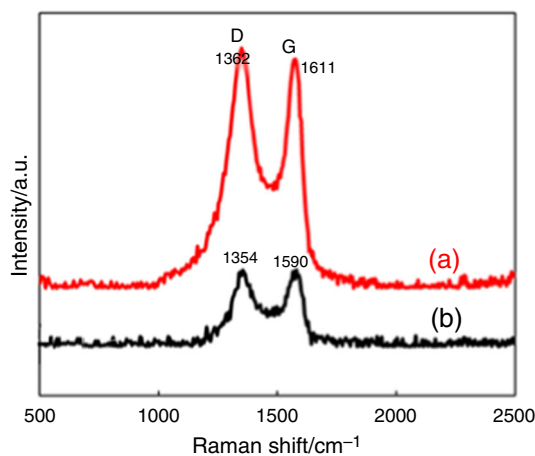
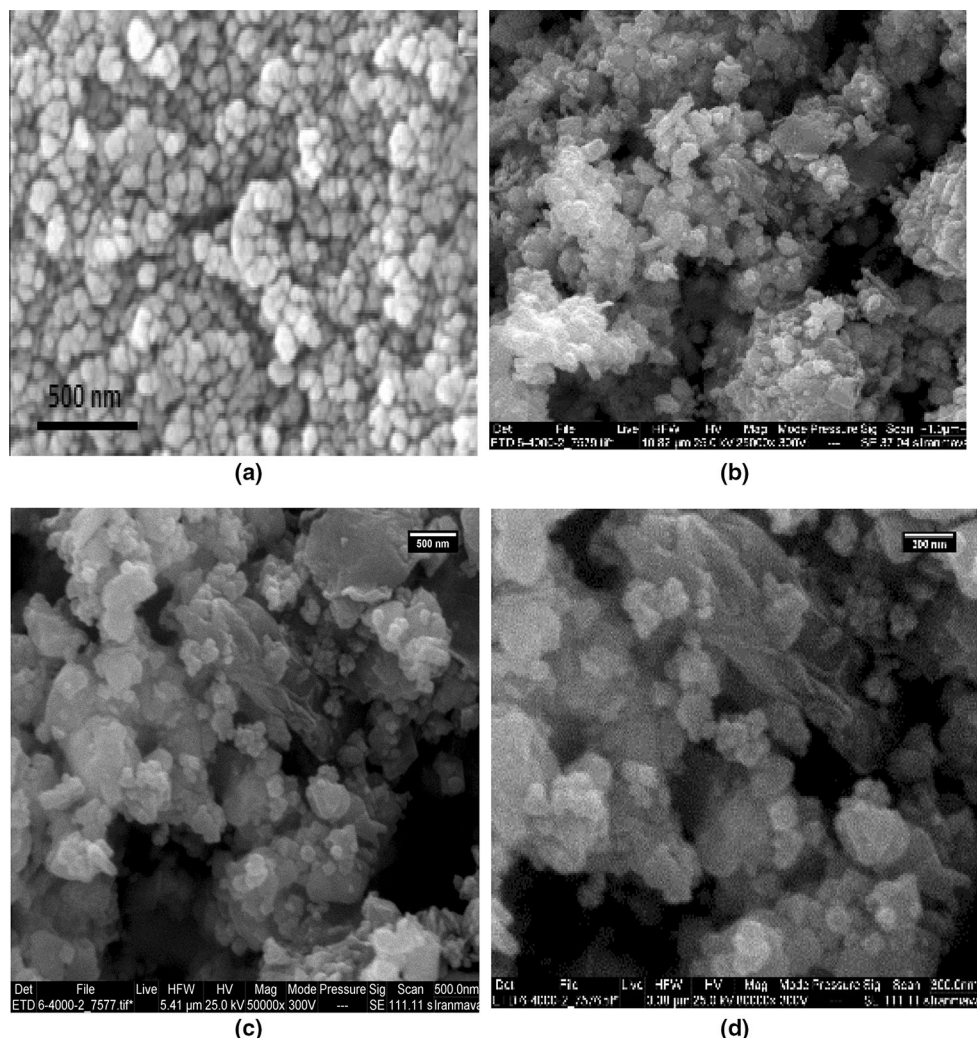


**Fig. 5** Raman spectra of GA (a) and CCO@GA nanocomposite (b)

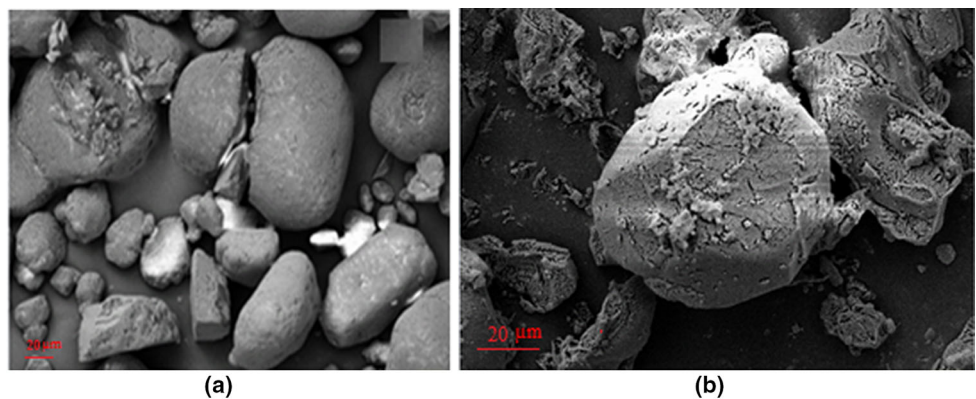
the reduction in oxidation groups in the CCO@GA nanocomposite during the heat treatment. Furthermore, the Brunauer–Emmett–Teller (BET) method is employed to

estimate the specific surface area of the CCO@GA. The data obtained from the nitrogen adsorption/desorption isotherm revealed that the BET specific surface area of CCO and CCO@GA nanocomposites was calculated to be 60.1 and 174.8 m<sup>2</sup> g<sup>-1</sup>, respectively. In comparison with CCO nanoparticles, the high specific surface area of the CCO@GA nanocomposites can provide more catalytic activity sites, indicating the good quality of GA as support with high surface area.

#### Characterization of AP + CCO@GA nanocomposite

The morphology and structure of pure AP and a representative AP/CCO sample were characterized by FE-SEM and are shown in Fig. 6. Figure 6a shows that the surface of pure AP was nearly uniform and the particle size of AP changed within 60–100 μm. Also, the FE-SEM image of AP/CCO nanocomposite (Fig. 6b) revealed that CuCr<sub>2</sub>O<sub>4</sub> spinel nanoparticle is deposited and coated homogeneously

**Fig. 6** FE-SEM images of pure AP particles (**a**) and AP + 4 mass% CCO nanocomposite (**b**)

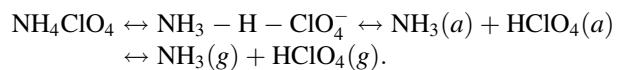


on the surface of AP and there is some agglomeration and their average particle size changed between 70 and 110  $\mu\text{m}$ . Also, the FE-SEM results along with related EDS spectra of AP/CCO@GA nanocomposite prepared by simple mixing and solvent–non-solvent are shown in Fig. 7. Figure 7a, b shows that in the solvent–non-solvent method, CCO@GA were deposited on the surface of AP in a uniform and complete way. Also, it is shown in EDS spectra of CCO@GA (Fig. 7c), the content of copper and chromium is about 4.2 by mass, and the content of carbon is about 16. However, CCO@GA in a simple mixture sample showed aggregated coating on the surface of AP (Fig. 7d, e). Moreover, in corresponding EDS spectra of CCO@GA (Fig. 7f), the content of copper and chromium is about 2.1 by mass, and the content of carbon is about 12. It is clear that the dispersion of CCO@GA nanocomposite in CCO@GA/AP nanocomposites is better than that in the mixed simply sample. This can be discussed as follows: (1) in the solvent/non-solvent process, firstly CCO@GA nanocomposites were dispersed well in non-solvent under ultrasonic, and next the well-dispersed CCO@GA nanocomposites were coated by AP; (2) the newly formed AP particles stabilized CCO@GA nanoparticles and inhibited them from accumulation.

### Catalytic activities of CCO NPs and AP + CCO@GA nanocomposite

The effect of the as-synthesized material was estimated by the thermogravimetric and differential scanning calorimetric (TG-DSC) technique. The DSC curve of pure AP is shown in Fig. 8. Pure AP shows the first endothermic peak at about 244 °C, which ascribed to the crystallographic transformation of AP from orthorhombic to a cubic structure. The cubic structure of AP accelerates the thermal decomposition due to the existence of crystal defects and dense packing. Moreover, there are two exothermic peaks, at the temperature of 290 and 432 °C, which are associated

with the low- (LTD) and high-temperature decomposition (HTD) of AP. The LTD process of AP decomposition (300–330) takes place as follows [39]:



According to the electron transfer theory, the LTD stage is assigned to the partial decomposition of AP and decomposition of AP into  $\text{NH}_4^+$  and  $\text{ClO}_4^-$ , which subsequently electron transfer from  $\text{ClO}_4^-$  to  $\text{NH}_4^+$  produce perchloric acid ( $\text{HClO}_4$ ) and ammonia ( $\text{NH}_3$ ), respectively. Since the Cu–Cr–O has unoccupied valence orbitals and defects on the crystal lattice, which results in trapping of electron from materials with additional electrons and involving in the electron transfer [40].

In general, the catalytic effect of various additives on thermal decomposition of AP is aimed to improve the released heat and reduce the temperatures of LTD and HTD.

The DSC results, as summarized in Table 1, show that the decomposition temperature of AP with 4% addition of  $\text{CuCr}_2\text{O}_4$  spinel NPs, simple mixing  $\text{CuCr}_2\text{O}_4@\text{GA}$  and  $\text{CuCr}_2\text{O}_4@\text{GA}$  prepared by solvent–non-solvent decreased by 92, 100 and 109 °C, respectively. Moreover, in all above samples merged the two exothermic peaks into one peak and greatly reduced the high-temperature decomposition peak. Furthermore, evaluation of the results demonstrates that AP/ $\text{CuCr}_2\text{O}_4@\text{GA}$  nanocomposites prepared by the solvent–non-solvent method have a better catalytic influence on the reduction in HTD temperature and enhancing the released heat than AP/ $\text{CuCr}_2\text{O}_4@\text{GA}$  prepared by simple mixing. Therefore, it can be seen that the enhancement of the released heat for AP with  $\text{CuCr}_2\text{O}_4@\text{GA}$  is much higher than pure AP (590 J g<sup>-1</sup>), suggesting the composite processing and GA as a support not only affect the decomposition temperature of ammonium perchlorate particles, but also cause a significant alteration in decomposition reaction enthalpy. Since nature, particle

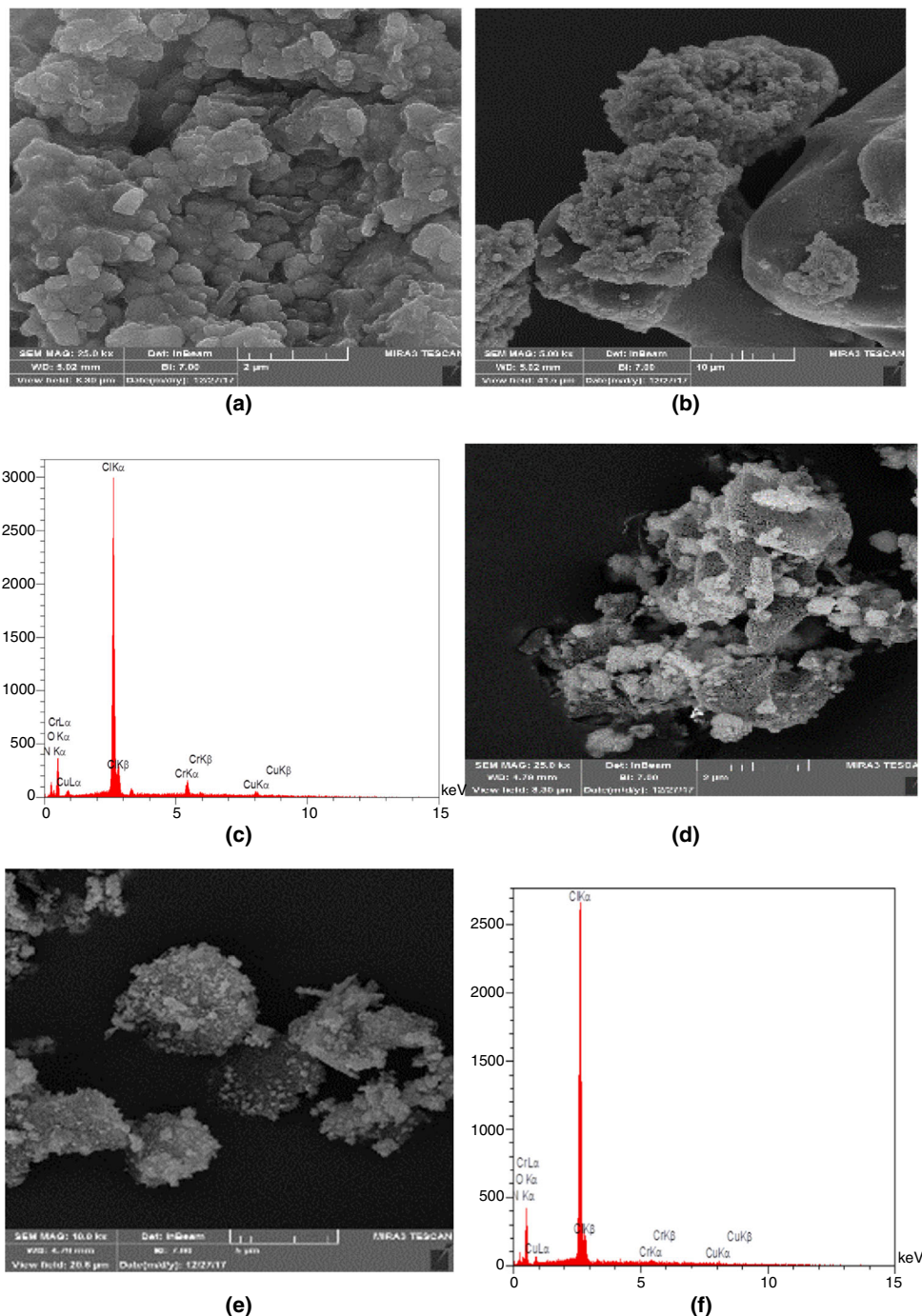


**Fig. 7** FE-SEM images and EDS results of AP + 4 mass% CCO@GA nanocomposites: prepared by solvent–non-solvent (**a–c**) and prepared by simple mixing methods (**d–f**)

size, ratio and way of mixing of catalyst to AP are the important parameters that influence highly the thermal decomposition of AP. Thus, the larger interfacial surface of  $\text{CuCr}_2\text{O}_4@\text{GA}$  and AP and better dispersion of  $\text{CuCr}_2\text{O}_4@\text{GA}$  in  $\text{CuCr}_2\text{O}_4@\text{GA}/\text{AP}$  nanocomposites can be the important reasons for the enhancement of catalytic activity of  $\text{CuCr}_2\text{O}_4@\text{GA}$  nanocomposite. In the range from room

temperature to 600 °C, the TG curve of pure AP displayed two mass loss steps. The initial mass loss of about 30% can be assigned to the partial decomposition of AP in the first step (LTD) where a well-known multiphase process produces  $\text{NH}_3$  and  $\text{HClO}_4$ . Also, alone GA has no considerable catalytic influence on thermal decomposition of AP and decrease the mass loss temperature only 17 °C, while only

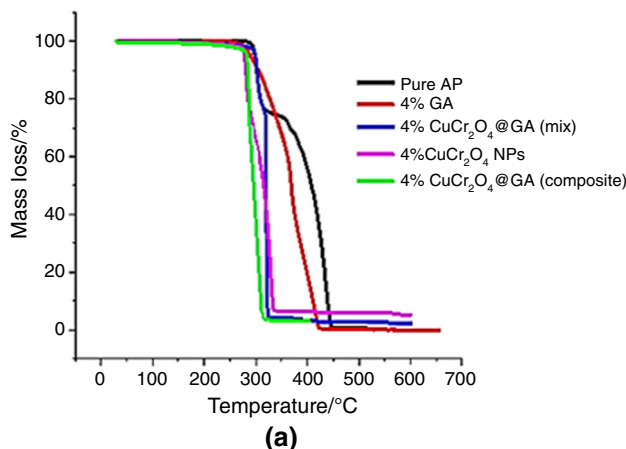


**Fig. 8** TGA (a) and DSC (b) curves of AP and AP composites in the presence of 4 mass% of different additives. Sample mass 3.0 mg; heating rate 10 °C min<sup>-1</sup> and air atmosphere

**Table 1** Results of AP thermal decomposition in the presence of 4 mass% of CuCr<sub>2</sub>O<sub>4</sub> NPs, GA and CuCr<sub>2</sub>O<sub>4</sub>@GA ( $\beta = 10 \text{ }^{\circ}\text{C min}^{-1}$ )

No.	Sample	mass%	Peak $T_m$ /°C		$\Delta H/\text{J g}^{-1}$
			LTD/°C	HTD/°C	
1	AP	100	297	432	590
2	AP/CuCr <sub>2</sub> O <sub>4</sub>	96/4	364	415	890
3	AP/GA	96/4	—	340	1181
4	AP/CuCr <sub>2</sub> O <sub>4</sub> @GA (M <sup>a</sup> )	96/4	—	332	1416
5	AP/CuCr <sub>2</sub> O <sub>4</sub> @GA (C <sup>b</sup> )	96/4	—	323	1760

<sup>a</sup>Mixing, <sup>b</sup>composite processing

**Table 2** Catalytic activities of some graphene-based nanocatalysts on the thermal decomposition of AP

No.	Sample	mass%	Peak $T_m$ /°C		$\Delta H/\text{J g}^{-1}$	Refs.
			LTD/°C	HTD/°C		
1	Nitrated graphene oxide	—	—	—	3236	[42]
2	Gr-MnOOH	2	—	334	—	[43]
3	Cu-Cr-O-TiO <sub>2</sub> /reduced graphene oxide	5	294	317	—	[44]
4	Co <sub>3</sub> O <sub>4</sub> /graphene oxide	2	—	297	1591	[45]
5	Graphene/Fe <sub>2</sub> O <sub>3</sub> aerogel	9	—	340.8	—	[46]
6	Graphene/Ni aerogel	5	—	368	—	[47]
7	AP/CuCr <sub>2</sub> O <sub>4</sub> @GA	4	—	323	1760	This research

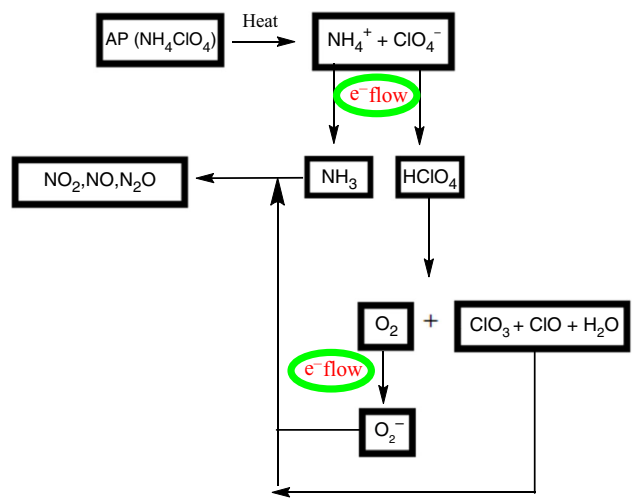


**Fig. 9** Schematic representation of thermal decomposition process of AP by CCO@GA nanocomposite

one mass loss step is observed for other nanocomposites, in agreement with the above DSC results. It can be observed from the available experimental results that the presence of the GA in CuCr<sub>2</sub>O<sub>4</sub>@GA nanocomposites enhances both the low-temperature and high-temperature processes and increases the exothermic heat released from the decomposition of AP. This behavior has been well related to the excellent electrical and thermal conductivity properties of GA, and this leads to faster movement of electrons in GA than among metal atoms.

Moreover, electrons can flow long distances without scattering in GA [41]. As shown in Fig. 9, according to the electron transfer theory, the electron transfer from  $\text{ClO}_4^-$

to  $\text{NH}_4^+$  produces  $\text{NH}_3$  and  $\text{HClO}_4$ , respectively. Then  $\text{O}_2$  that is produced from  $\text{HClO}_4$  transformed to superoxide ion ( $\text{O}_2^-$ ). Therefore, in the presence of GA as support for CCO NPs, the flow of electrons accelerated, and consequently, the above two controlling steps for thermal decomposition of AP speed up. The products from the decomposition of  $\text{HClO}_4$  and the superoxide ion can help the decomposition of  $\text{NH}_3$  and complete the decomposition of AP. Also, the large theoretical surface area of GA ( $\sim 530 \text{ m}^2 \text{ g}^{-1}$ ) leading to the CCO@GA nanocomposite provides more active sites to absorb gas-phase molecules for the catalysis. Pure CCO NPs are easily aggregated and show fewer active sites. Table 2 [42–47] compares the catalytic activity results of nanocatalysts supported on graphene and its derivatives on the thermal decomposition of AP. Comparison of the obtained data showed that among derivatives of graphene, GAs as support of additives appears further lower the peak of high-temperature decomposition and improve heat release of thermal decomposition of AP.

## Conclusions

In this work,  $\text{CuCr}_2\text{O}_4$  nanoparticles with 42 nm particle size and  $\text{CuCr}_2\text{O}_4@\text{GA}$  nanocomposite were prepared by simple hydrothermal method and calcination processes. Characterization results exhibited that the  $\text{CuCr}_2\text{O}_4$  NPs with spherical shape deposited uniformly on GA. The as-prepared  $\text{CuCr}_2\text{O}_4@\text{GA}$  composites revealed high catalytic activity for thermal decomposition of AP. The TG-DSC analysis showed that  $\text{CuCr}_2\text{O}_4@\text{GA}/\text{AP}$  nanocomposite prepared by solvent–non-solvent method compared with the simply mixed sample and alone  $\text{CuCr}_2\text{O}_4$  NPs had higher catalytic activity on the thermal decomposition of AP.

## References

- Zhi J, Tian-Fang W, Shu-Fen L, Feng-Qi Z, Zi-Ru L, Cui-Mei Y, Yang L, Shang-Wen L, Gang-Zhui Z. Thermal behavior of ammonium perchlorate and metal powders of different grades. *J Therm Anal Calorim.* 2006;85:315–20.
- Juibari NM, Eslami A. Investigation of catalytic activity of  $\text{ZnAl}_2\text{O}_4$  and  $\text{ZnMn}_2\text{O}_4$  nanoparticles in the thermal decomposition of ammonium perchlorate. *J Therm Anal Calorim.* 2017;128:115–24.
- Chen LJ, Li GS, Li LP. CuO nanocrystals in thermal decomposition of ammonium perchlorate: stabilization, structural characterization and catalytic activities. *J Therm Anal Calorim.* 2008;91(2):581–7.
- Singh G, Kapoor I, Dubey S, Siril PF. Preparation, characterization and catalytic activity of transition metal oxide nanocrystals. *J Sci Conf Proc.* 2009;1:11–7.
- Viswanath JV, Vijayadarshan P, Mohan T, Srinivasa RNV, Gupta A, Venkataraman A. Copper chromite as ballistic modifier in a typical solid rocket propellant composition: a novel synthetic route involved. *J Energ Mat.* 2018;36:69–81.
- Zheng S, Liu J, Wang Y, Li F, Xiao L, Ke X, Lan Z. Effect of aluminum morphology on thermal decomposition of ammonium perchlorate. *J Therm Anal Calorim.* 2018;134:1823–8.
- Hosseini SG, Toloti SJH, Babaei K, Ghavi A. The effect of average particle size of nano- $\text{Co}_3\text{O}_4$  on the catalytic thermal decomposition of ammonium perchlorate particles. *J Therm Anal Calorim.* 2016;124:1243–54.
- Juibari NM, Tarighi S.  $\text{MnCo}_2\text{O}_4$  nanoparticles with excellent catalytic activity in thermal decomposition of ammonium perchlorate. *J Therm Anal Calorim.* 2018;2018:1–10.
- Ping C, Li F, Jian Z, Wei J. Preparation of Cu/CNT composite particles and catalytic performance on thermal decomposition of ammonium perchlorate. *Propellants Explos Pyrotech.* 2006;31:452–5.
- Said A. The role of copper-chromium oxide catalysts in the thermal decomposition of ammonium perchlorate. *J Therm Anal Calorim.* 1991;37(5):959–67.
- Hosseini SG, Alavi MA, Ghavi A, Toloti SJ, Agend F. Modeling of burning rate equation of ammonium perchlorate particles over Cu–Cr–O nanocomposites. *J Therm Anal Calorim.* 2015;119(1):99–109.
- Acharyya SS, Ghosh S, Adak S, Tripathi D, Bal R. Fabrication of  $\text{CuCr}_2\text{O}_4$  spinel nanoparticles: a potential catalyst for the selective oxidation of cycloalkanes via activation of C sp<sup>3</sup>–H bond. *Catal Commun.* 2015;59:145–50.
- Royn S, Ghose J. Syntheses and studies on some copper chromite spinel oxide composites. *Mater Res Bull.* 1999;34:1179–86.
- Armstrong RW, Baschung B, Booth DW, Samirant M. Enhanced propellant combustion with nanoparticles. *Nano Lett.* 2003;3:253–5.
- Kawamoto AM, Pardini LC, Rezende LC. Synthesis of copper chromite catalyst. *Aerospace Sci Technol.* 2004;8:591–8.
- Rajeev R, Devi KA, Abraham A, Krishnan K, Krishnan TE, Ninan KN, Nair CGR. Thermal decomposition studies. Part 19. Kinetics and mechanism of thermal decomposition of copper ammonium chromate precursor to copper chromite catalyst and correlation of surface parameters of the catalyst with propellant burning rate. *Thermochim Acta.* 1995;254:235–47.
- Hosseini SG, Abazari R, Gavi A. Pure  $\text{CuCr}_2\text{O}_4$  nanoparticles: synthesis, characterization and their morphological and size effects on the catalytic thermal decomposition of ammonium perchlorate. *Solid State Sci.* 2014;37:72–9.
- Yuan Y, Jiang W, Wang Y, Shen P, Li F, Li P, Zhao F, Gao H. Hydrothermal preparation of  $\text{Fe}_2\text{O}_3$ /graphene nanocomposite and its enhanced catalytic activity on the thermal decomposition of ammonium perchlorate. *Appl Surf Sci.* 2014;303:354–9.
- Liu JX, Li FS, Jiang W, Guo XD, Liu GP. Effects of nano NiO/CNTs and  $\text{Co}_3\text{O}_4$ /CNTs on thermal decomposition of AP and HTPB/AP propellant. *J Solid Rocket Technol.* 2007;20:243–7.
- Liu P, Kong JR, Xu XD, Sun FL, Liu QC. Preparation and catalytic activity of  $\text{Fe}_2\text{O}_3$ /CNT to thermal decomposition of ammonium perchlorate. *Adv Mater Res.* 2012;396:837–40.
- Zhu J, Zeng G, Nie F, Xu X, Chen S, Han Q, Wang X. Decorating graphene oxide with CuO nanoparticles in a water-isopropanol system. *Nanoscale.* 2010;2:988–94.
- Zhao J, Liu Z, Qin Y, Hu W. Fabrication of  $\text{Co}_3\text{O}_4$ /Graphene Oxide composites using supercritical fluid and their catalytic application for the decomposition of ammonium perchlorate. *CrystEngComm.* 2014;16:2001–8.
- Chen J, He S, Huang B, Zhang L, Qiao Z, Wang J, Hao Q. Highly space-confined ammonium perchlorate in three-dimensional

- hierarchically ordered porous carbon with improved thermal decomposition properties. *Appl Surf Sci.* 2018;457:508–15.
24. Wang X, Li J, Luo Y, Huang M. A novel ammonium perchlorate/graphene aerogel nanostructured energetic composite: preparation and thermal decomposition. *Sci Adv Mater.* 2014;6:530–7.
  25. Zhang X, Sui Z, Xu B, Yue S, Luo Y, Zhan W, Liu B. Mechanically strong and highly conductive graphene aerogel and its use as electrodes for electrochemical power sources. *J Mater Chem.* 2011;18:6494–7.
  26. Chen W, Yan L. In situ self-assembly of mild chemical reduction graphene for three-dimensional architectures. *Nanoscale.* 2011;3:3132–7.
  27. Worsley MA, Pauzauskis PJ, Olson TY, Biener J, Satcher JH Jr, Baumann TF. Synthesis of graphene aerogel with high electrical conductivity. *J Am Chem Soc.* 2010;40:4067–9.
  28. Lan YF, Jin MM, Luo YJ. Preparation and characterization of graphene aerogel/Fe<sub>2</sub>O<sub>3</sub>/ammonium perchlorate nanostructured energetic composite. *J Sol-Gel Sci Technol.* 2015;74:161–7.
  29. Chen LJ, Li GS, Qi P, Li LP. Thermal decomposition of ammonium perchlorate activated via addition of NiO nanocrystals. *J Therm Anal Calorim.* 2008;92:765–9.
  30. Ma Z, Li F, Bai H. Effect of Fe<sub>2</sub>O<sub>3</sub> in Fe<sub>2</sub>O<sub>3</sub>/AP composite particles on thermal decomposition of AP and on burning rate of the composite propellant. *Propellants Explos Pyrotech.* 2006;31:447–51.
  31. Abbas E, Nafise MJ, Hosseini SG. Fabrication of ammonium perchlorate/copper chromium oxides core-shell nanocomposites for catalytic thermal decomposition of ammonium perchlorate. *Mater Chem Phys.* 2016;181:12–20.
  32. Hosseini SG, Ahmadi R, Ghavi A, Kashi A. Synthesis and characterization of  $\alpha$ -Fe<sub>2</sub>O<sub>3</sub> mesoporous using SBA-15 silica as template and investigation of its catalytic activity for thermal decomposition of ammonium perchlorate particles. *Powder Technol.* 2015;278:316–22.
  33. Wang JX, Zhang WC, Zheng ZL, Gao Y, Ma KF, Ye JH, Yang Y. Enhanced thermal decomposition properties of ammonium perchlorate through addition of 3DOM core-shell Fe<sub>2</sub>O<sub>3</sub>/Co<sub>3</sub>O<sub>4</sub> composite. *J Alloys Compd.* 2017;724:720–7.
  34. Hosseini SG, Khodadadipoor Z, Mahyari M. CuO nanoparticles supported on three dimensional nitrogen-doped graphene as promising catalyst for thermal decomposition of ammonium perchlorate. *Appl Organomet Chem.* 2018;32:e3959.
  35. Hosseini SG, Gholami S, Mahyari M. Highly dispersed Ni–Mn bimetallic nanoparticles embedded in 3D nitrogen-doped graphene as an efficient catalyst for the thermal decomposition of ammonium perchlorate. *New J Chem.* 2018;42:5889–99.
  36. Acharyya SS, Ghosh S, Adak S, Sasaki T, Bal R. Facile synthesis of CuCr<sub>2</sub>O<sub>4</sub> spinel nanoparticles: a recyclable heterogeneous catalyst for the one pot hydroxylation of benzene. *Catal Sci Technol.* 2014;12:4232–41.
  37. Jr Hummers, William S, Offeman RE. Preparation of graphitic oxide. *J Am Chem Soc.* 1958;80:1339–1339.
  38. Birks LS, Friedman H. Particle size determination from X-ray broadening. *J Appl Phys.* 1946;17:687–92.
  39. Boldyrev VV. Thermal decomposition of ammonium perchlorate. *Thermochim Acta.* 2006;443:1–36.
  40. Eslami A, Juibari NM, Hosseini SG. Fabrication of ammonium perchlorate/copper-chromium oxides core-shell nanocomposites for catalytic thermal decomposition of ammonium perchlorate. *Mater Chem Phys.* 2016;181:12–20.
  41. Geim AK, Novoselov KS. The rise of graphene. *Nat Mater.* 2007;6:183–91.
  42. Zhang W, Luo Q, Duan X, Zhou Y, Pei C. Nitrated graphene oxide and its catalytic activity in thermal decomposition of ammonium perchlorate. *Mater Res Bull.* 2014;50:73–8.
  43. Chen S, Zhu J, Huang H, Zeng G, Nie F, Wang X. Facile solvothermal synthesis of graphene–MnOOH nanocomposites. *J Solid State Chem.* 2010;183:2552–7.
  44. Kumar H, Tengli PN, Mishra VK, Tripathi P, Bhushan A, Mishra PK. The effect of reduced graphene oxide on the catalytic activity of Cu–Cr–O–TiO<sub>2</sub> to enhance the thermal decomposition rate of ammonium perchlorate: an efficient fuel oxidizer for solid rocket motors and missiles. *RSC Adv.* 2017;7:36594–604.
  45. Zhao J, Liu Z, Qin Y, Hu W. Fabrication of Co<sub>3</sub>O<sub>4</sub>/graphene oxide composites using supercritical fluid and their catalytic application for the decomposition of ammonium perchlorate. *CrystEngComm.* 2014;16:2001–8.
  46. Lan Y, Li X, Li G, Luo Y. Sol-gel method to prepare graphene/Fe<sub>2</sub>O<sub>3</sub> aerogel and its catalytic application for the thermal decomposition of ammonium perchlorate. *J Nanopart Res.* 2015;17:395.
  47. Lan Y, Jin B, Deng J, Luo Y. Graphene/nickel aerogel: an effective catalyst for the thermal decomposition of ammonium perchlorate. *RSC Adv.* 2016;6:82112–7.

**Publisher's Note** Springer Nature remains neutral with regard to jurisdictional claims in published maps and institutional affiliations.